ERBB2 drives YAP activation and EMT-like processes during cardiac regeneration

Alla Aharonov[1], Avraham Shakked[1], Kfir Baruch Umansky[1], Alon Savidor[2] , David Kain[1], Daria Lendengolts[1], Or-Yam Revach[1], Yuka Morikawa[3], Jixin Dong[4], Yishai Levin[2], Benjamin Geiger[1], James F. Martin[5] and Eldad Tzahor*[1]

[1]Department of Molecular Cell Biology, Weizmann Institute of Science, Rehovot, 7610001, Israel.

[2]The De Botton Protein Profiling institute of the Nancy and Stephen Grand Israel National Center for Personalized Medicine, Weizmann Institute of Science, Rehovot, 7610001, Israel.

[3]The Texas Heart Institute Cardiomyocyte Renewal Lab, Houston, Texas, 77030, USA.

[4] Eppley Institute for Research in Cancer, Fred & Pamela Buffett Cancer Center, University of Nebraska Medical Center, Omaha 68198, NE, USA.

[5] Department of Molecular Physiology and Biophysics, Baylor College of Medicine, and The Texas Heart Institute Cardiomyocyte Renewal Lab, Houston, Texas, 77030, USA.

*Correspondence: eldad.tzahor@weizmann.ac.il

Abstract

Cardiomyocyte (CM) loss after injury results in adverse remodelling and fibrosis, which inevitably lead to heart failure. ERBB2-Neuregulin and Hippo-YAP signaling pathways are key mediators of CM proliferation and regeneration, yet the crosstalk between these pathways is unclear. Here, we demonstrate in adult mice that transient over-expression (OE) of activated ERBB2 in CMs promotes cardiac regeneration in a heart failure model. OE CMs present an EMT-like regenerative response manifested by cytoskeletal remodelling, junction dissolution, migration, and ECM turnover. Molecularly, we identified YAP as a critical mediator of ERBB2 signaling. In OE CMs, YAP interacts with nuclear envelope and cytoskeletal components, reflecting the altered mechanic state elicited by ERBB2. Hippo-independent activating phosphorylation on YAP at S352 and S274 were enriched in OE CMs, peaking during metaphase, and viral overexpression of YAP phospho-mutants dampened the proliferative competence of OE CMs. Taken together, we demonstrate a potent ERBB2-mediated YAP mechanosensory signaling, involving EMT-like characteristics, resulting in heart regeneration.

Main Text

Adult mammalian cardiomyocytes (CMs) have poor proliferative and consequently regenerative potential after injury. The inability to replace the lost contractile units after acute myocardial infarction (MI) is paralleled by scarring at the injured area[1]. The aftermath of an acute MI inevitably leads to permanent loss of contractile force, which gradually progresses into heart failure (HF) and death. A robust regenerative response, however, was demonstrated in adult hearts of lower vertebrates such as zebrafish[2] and even in neonatal mammalian hearts during a short time window after birth[3]. For both mammalian and lower vertebrates, the source of newly formed CMs was traced to pre-existing CMs, and was shown to involve CM dedifferentiation and cell cycle re-entry[3,4], which fuels the field of cardiac regeneration to investigate CM cell-cycle regulation[5,6]. Although CM proliferation is a pre-requisite for cardiac regeneration, it has to be coordinated with other overarching processes. CM migration and ECM replacement during zebrafish heart regeneration outline the coordinated effort of multiple biological processes needed for successful regeneration[7].

Neuregulin-1 (Nrg1), and its tyrosine kinase receptors ERBB4 and ERBB2 network are critical for CM proliferation and function prenatally and postnatally[8]. In mice, we demonstrated that ERBB2 levels in CMs decline after birth, resulting in CM cell cycle arrest and loss of cardiac regenerative potential. ERBB2 is necessary for the proliferative response of CMs induced by NRG1 during embryonic and neonatal stages, and sufficient to trigger a robust regenerative response following MI in adult mice (using a CM-restricted inducible overexpression of constitutively active *Erbb2* isoform, ca*Erbb2*-cOE, OE in short)[9]. Similarly, inhibition of Erbb2 in zebrafish, disrupts CM proliferation and heart regeneration[10], and NRG1 promotes CM cycling only in an early time frame when applied to human neonatal CMs *in vitro*[11].

The Hippo pathway is an important negative regulator of the cell cycle in CMs[12,13]. Hippo-YAP signaling has been investigated in cardiac biology via loss-of-function (cKO) and gain-of function approaches. Multiple lines of evidence point to the essential roles of YAP in CM proliferation and cardiac regeneration[14,15,16,17,18,19,20]. The effects of Hippo pathway inhibition and ERBB2 activation both result in CM dedifferentiation and proliferation as well as cardiac regeneration. Whether these two pathways act independently in cardiac regeneration or are interconnected, and precisely how, is unclear.

Alongside the Hippo pathway, mechanotransduction robustly regulates YAP activity in an integrative manner[21,22]. Mechanotransduction is the relay of mechanical stimuli to biochemical cues, transduced by the cytoskeleton. Altered cellular shape, connectivity and

adhesion, actin dynamics, and the continuum between the cytoskeleton and the nucleus via the 'Linker of Nucleoskeleton and Cytoskeleton' complex (LINC complex), are all implicated in mechanotransduction signaling. Numerous studies demonstrated a Hippo-independent YAP regulation, highlighting a multifaceted control of YAP, especially in the heart[23,24,25].

Here we show that ERBB2-driven regeneration of scarred hearts recapitulates core-EMT processes in CMs, involving profound cytoskeletal alterations. YAP is activated and required downstream to ERBB2, via a signaling circuit involving remodeled cytoskeleton and nuclear envelope components, as well as Hippo-independent phosphorylation of Yap on S274 and S352.

Results

Delayed ERBB2 induction in an HF model triggers functional recovery, scar replacement and involves EMT-like processes in cardiomyocytes

We have previously shown that transient ERBB2 activation promotes robust cardiac regeneration in acute MI model in juvenile and adult mice[9]. In order to translate this regenerative signal into a more clinically-relevant model of HF, we examined cardiac regeneration in the context of pre-existing injury. Using the transient ca*Erbb2* CM-specific induction system[9], we designed an experiment in which adult mice underwent MI and >3 weeks after, ca*Erbb2* was induced. Heart injuries were similar in OE and WT littermates at the 3-weeks time point (Fig. 1A-E , fig. S1A). ca*Erbb2* was induced for 3 weeks, representing ~ 2.5 weeks of ERBB2 expression, and was consistently characterized by ventricular wall hypertrophy and lumen shrinkage, which resulted in a transient increase in ejection fraction (Fig. 1B-D green period, E, fig. S1B). During ca*Erbb2* induction, CMs undergo dedifferentiation, proliferation and hypertrophy[9] resulting in lower stroke volume and cardiac output values compared to WT mice (fig. S1C,D). Cessation of ERBB2 signaling by Doxycyclin (Dox) re-administration resulted in hypertrophy reversal and CM redifferentiation that lead to sustained improvement in numerous cardiac functional parameters (Fig. 1B-E, fig. S1B-D). In addition, functional improvement was accompanied by reduced scarring in OE hearts compared to WTs (Fig. 1F,G). Hence, delayed transient ERBB2 activation in CMs can trigger functional and structural regeneration in a mouse HF model.

To appreciate the underlying cellular characteristics of OE CMs, we performed bulk RNAseq

comparing injured WT and OE hearts. This analysis highlighted epithelial to mesenchymal transition (EMT) with the highest enrichment score (Fig. 1H, fig. S2A) among other hallmarks previously implicated in cardiac regeneration, such as hypoxia[26], angiogenesis[27,28] and glycolysis[29,30]. Although the myocardium is not an epithelial tissue, EMT-like behaviors such as ECM-deposition and degradation, and CM migration are in line with the requirements for tissue replacement and regeneration in the context of a pre-existing scar. We therefore tested several EMT-like processes in OE vs WT CMs. First, we examined ECM degradation using a functional fluorescent gelatin degradation assay in P7 cardiac cultures. Quantification revealed a strong degradation activity of the OE CMs compared to WTs (Fig. 1I-K). RNA expression of the major EMT-related MMPs was elevated in OE adult hearts compared to WTs (Fig. 1L). Examination of cluster EMT gene transcripts revealed an elevation in many EMT hallmark genes[31] (fig. S2B-E). In line with that, IF staining of heart sections revealed loss of CM connectivity and directionality in OE hearts, compared to the organized and tightly defined WT architecture (fig. S2F). We next investigated CM motility in P7 cardiac culture migration assay. OE CMs migrated into the gap area, possessing elongated morphology and remarkable cytoskeletal protrusions, unlike WT CMs that failed to move (Fig. 1M-Q). To deepen this investigation, we utilized time-lapse microscopy imaging of fluorescently-tagged OE/WT CMs with tdTomato (Movies S1, S2). Single-cell CM tracking revealed that OE CMs were more motile (and proliferative) (Fig. 1R,S). Staining for the mesenchymal, migration-associated intermediate filament protein vimentin revealed that OE CMs uniquely developed a vimentin-rich cytoskeleton which is distinct from the contractile acto-myosin sarcomere typical for WT CMs (Fig. 1T). Taken together, these findings demonstrate functional cardiac improvement following myocardial ERBB2 activation, in a pre-existing scar setting (aka HF model). Remarkably, CMs of regenerative OE hearts were characterized by EMT-like features such as migration and pronounced ECM remodeling during ERBB2 activation.

YAP is activated downstream to ERBB2 signaling in cardiomyocytes

To get a deeper insight into the mechanism of ERBB2-mediated regeneration we employed proteome and phospho-proteome analyses followed by mass-spectrometry, in addition to the RNAseq (Fig. 2A). Evaluation of predicted molecular regulators highlighted ERBB2 and various cell cycle regulators concomitant with the inhibition of tumor suppressors (Fig. 2B). This corroborates the model and is consistent with the proliferative nature of OE CMs. Interestingly, *Yap* and *Ctgf* (a target of YAP) were highlighted as upstream regulators in the

OE hearts (Fig. 2B). Clustering of differentially phosphorylated proteins into signaling networks identified several pathways, including actin cytoskeleton, RHOA, and Hippo. (Fig. 2C). Interestingly, actin dynamics and RHOA have been linked to YAP activation via mechanosensory mechanisms[22,32] while Hippo signaling is a potent canonical negative regulator of YAP[33.33]. Clustering of differentially expressed proteins highlighted terms associated with mitosis and heart development, further underscoring regenerative aspects (Fig. 2D). Considering the central role of YAP in CM proliferation[14,18,20] and cardiac regeneration[13,16], we sought to validate its involvement, and further explore ERBB2-YAP signal relay. Staining of heart sections revealed an enrichment in YAP nuclear accumulation in OE CMs (Fig. 2E,F), and overall elevated YAP levels in OE CMs (Fig. 2G,H). In line with this, qRT-PCR analysis of YAP target genes revealed robust YAP transcriptional signature in OE heart lysates (Fig. 2I).

No evidence for Hippo pathway attenuation in OE hearts

To evaluate Hippo pathway activity, we analyzed the phosphoproteomic dataset obtained from WT and OE heart lysates. Quantitative phosphoproteomics indicate increased Hippo activity in OE compared to WT heart lysates, concomitantly with proteomic data showing increased YAP and its targets CTGF and ANKRD1 (fig. S3A-C). Specifically, phosphorylation sites for Hippo pathway components MOB1A and MST2 were detected on activating sites which stimulate Hippo function[34] (fig. S3A,B). YAP S149 and S94, 2 of the 5 known LATS sites[35] were also detected as well as the canonic LATS site S89 on Taz (fig. S3A,B), further reflecting Hippo activity. WB validation revealed higher levels of several Hippo components in OE heart lysates, including LATS1 and LATS2 kinases (fig. S3D,E). In addition, the major negative phosphorylation site by LATS, YAP S112 (in mice, S127 in human) was also elevated in OE hearts, proportionally to YAP levels (fig. S3F,G). Taken together, these results do not suggest Hippo pathway silencing as a mechanism for the elevated YAP activity in ERBB2-OE hearts. Our interpretation of the data is that the active Hippo pathway acts as a negative feedback mechanism to restrain YAP activity.

YAP is required for ERBB2-related cardiac phenotypes

We went on to evaluate the requirement of YAP to the ERBB2-OE heart phenotype by creating a transgenic mouse of both ca*Erbb2* OE and *Yap* KO with independently-activated Tamoxifen (Tam) and Dox modules that are both CM-restricted and temporally controlled (Fig. 3A; mice that were both ca*Erbb2* OE and underwent Cre-mediated *Yap* excision termed OE-knockdown (OE-KD) (Fig. 3A). In order to determine whether YAP is required for

ERBB2 signaling, we compared the following 3 groups; WT, OE and OE-KD. The cardiac YAP KD was evaluated by expression of YAP target genes and YAP protein (Fig. 3B,C), showing reduced YAP protein and transcriptional signature levels. Echocardiographic analysis revealed that ERBB2-driven elevation of ejection fraction, myocardial wall thickening, and reduced systolic and diastolic volumes, were blunted in YAP OE-KD hearts, resulting in overall cardiac measurements between WT and OE hearts (Fig. 3D-H). The proliferation markers Ki67 and PH3 were reduced in OE-KD compared to OE CMs, indicating that YAP is required for ERBB2-mediated CM proliferation. The expression of prominent EMT marker genes were reduced in OE-KD hearts compared to the elevation seen in OE hearts (Fig. 3K). Finally, histological analysis revealed reduced tissue disarray and intercellular gaps in OE-KD hearts reflecting an intermediate stage between WT and OE groups (Fig. 3L). Taken together, these results demonstrate that YAP is indispensable for ERBB2 signaling outcomes in CMs.

Cardiomyocyte ERBB2 signaling induces an altered mechanical state

To gain insight into YAP signaling driven by ERBB2 activation, we employed an unbiased and quantitative Co-IP-MS analysis of YAP in OE and WT heart lysates, in order to identify YAP binding proteins (Fig. 4A, fig. S4A). Of these, we identified nuclear envelope, cytoskeletal, and nuclear binding partners enriched in OE hearts (Fig. 4B-D, fig. S4B). The majority of the nuclear interactors are histone proteins, consistent with the chromatin remodeling activity of YAP in the heart[17], corroborating YAP nuclear accumulation in OE CMs (Fig. 4D). The mechanosensitive actin binding protein, Flnc and associated proteins, Hspb7 and Xirp2, were enriched binding partners in OE hearts (Fig. 4C), the latter being implicated also in mechanotransduction[36,37,38]. YAP interaction with the intermediate filament protein Nestin was elevated in OE hearts. Nestin, a characteristic component of embryonic CMs, was also shown to correlate with YAP activation in fetal CMs[39]. Finally, the nuclear envelope proteins Sun1, Sun2 (both part of the LINC complex), Tor1aip1, Tmpo and LaminA/C were enriched YAP interactors in OE hearts. These proteins, implicated in nuclear mechanosensing, form a complex at the inner nuclear membrane (INM) with other LINC components (Fig. 4E)[40].

Given the substantial involvement of YAP mechanosensory fingerprints in the Co-IP-MS assay, we focused on the differences in mechanical properties of OE and WT hearts, starting with the nucleus, the main mechanosensing organelle. Nuclear projected area was elevated in OE CMs mostly in the transverse axis, suggesting that OE nuclei experience more

mechanical stress (Fig. 4F-H)[41]. Consistently, Lamin A/C levels in OE hearts were elevated (Fig. 4I), also known as "stress strengthening" positive feedback that withstands forces and protects nuclei experiencing formidable mechanical strain against fragility[42,43]. Lamin A/C phosphorylation on S22 was also elevated in OE hearts (Fig. 4I). This mechanosensitive phosphorylation was shown to promote Lamin A solubilization into the nucleoplasm and is associated with mitotic NEBD[44]. Likewise, analysis of the proteome revealed an elevation in several cytoplasmic membrane-bound and nuclear-envelope bound force sensors and transducers in OE hearts (Fig. 4J).

The cytoskeleton of OE CMs was substantially enriched with Nestin at the expense of the striated sarcomeric protein cTNI. WT CMs, conversely, displayed organized, striated sarcomeres as evidenced by cTNI staining (Fig. 4K, insets, fig. S5A,B). The major intercalated disk gap junction protein Gja1, which is required for proper mechanical and electrical coupling between CMs[45] was downregulated and displaced in OE CMs (Fig. 4L, fig. S5C,D). Finally, assessing the microtubule network (required for mitosis) reveled a striking increase in microtubules in OE CMs, as well as elevation of dTyr tubulin, a PTM on tubulin that hampers sarcomeric contractility (Fig. 4M, fig. S5E,F)[46]. Taken together, these findings indicate that all three cytoskeletal networks of OE CMs (microfilaments, intermediate filaments and microtubules) were remodeled following ERBB2 activation, thus shifting the CMs from contractility to force sensing and regulating function, and suggests the substitution of the lateral contractile force propagation in WT CMs to a nuclear directed force in OE CMs (Fig. 4N).

YAP phosphorylation on S274 and S352 peaks during metaphase, and is required for cell division

To further deepen our understanding of YAP regulation elicited by ERBB2 activation, we focused on (non-Hippo) phosphorylation sites of YAP at S274 (S289 in human) and S352 (S367 in human) detected in our phosphoproteomics and YAP IP-MS profiling. Using a custom-made antibody against pYAP S274[47] and a newly generated custom antibody against pYAP S352, we validated the enrichment of these YAP phospho-forms in OE heart sections (Fig. 5A,B). In OE adult CMs *in vivo* pYAP S274 demonstrated a diverse pattern localizing mostly to cytoskeletal compartments, but also perinuclear and nuclear (Fig. 5A), while pYAP S352 was strongly nuclear. Both pYAP S274 and pYAP S352 were present to some extent in intercalated discs, as shown before for general YAP[48,49]. Levels of pYAP on S274 and S352 measured by WB, similarly showed elevation in OE heart lysates (fig. S6A,B). Interestingly,

in addition to the typical YAP protein, we identified and validated a lower molecular weight isoform of YAP, which is mostly detected by antibodies to phospho-YAP S274/S352, to be enriched in OE CMs (fig. S6A-F).

IF analysis on P7 cardiac cultures with anti pYAP S274 antibody revealed that while all cultured fixed cells have some level of nuclear staining, pYAP S274 in OE CMs had a strong filamentous appearance, as well as perinuclear and nuclear, which peaked during mitosis throughout the cell (fig. S6G). Likewise, pYAP S352 staining in cardiac cultures peaks throughout the cell during mitosis (condensed chromatin), and otherwise was enriched in the nuclei of OE CMs (fig. S6H). This expression pattern recapitulates the mitosis pattern observed in non-CMs for pYAP S274 (fig. S6 G,H, insets in WT)[47]. Co-staining of the mitosis marker Aurora kinase B (Aurkb) validated that pYAP S274 and S352 peak during mitosis (Fig. 5C,D and fig. S6I,J). Intensified staining was seen during metaphase, during which all CMs were double positive (in existence, not localization) for Aurkb and pYAP S274 or pYAP S352. We noted a gradual reduction of pYAP S274 and S352 staining with the progression of mitosis, which was lowest during cytokinesis (Fig. 5C,D and fig. S6I-K). In order to determine whether pYAP S274 and S352 characterize dividing CMs during normal development, we stained embryonic E16.5 WT hearts and detected a strong nuclear pYAP S274 and S352 staining that peaks during chromosome condensation. Co-staining with Aurkb demonstrated that these were CMs undergoing metaphase, and the staining was mostly diminished upon cytokinesis completion (Fig. 5E, fig. S6L).

We next examined pYAP S274 expression patterns in hearts over-expressing a constitutively active form of YAP (YAP5SA) rendering it immune to inhibition by the Hippo pathway[17]. Similarly to OE hearts *in vivo*, YAP 5SA CMs displayed a peak of both pYAP S274 and S352 during metaphase (Fig. 5F,G and fig. S8M), although YAP5SA CMs lacked the prominent pYAP S274 cytoskeletal pattern observed in OE hearts. Finally, we evaluated the requirement of the two YAP phosphorylation sites, S274 and S352, for mitosis, by infecting P7 OE/WT cardiac cultures with AAV harboring serine-to-alanine YAP phosphomutants in both sites separately and together (YAP2A), and analyzed their proliferative potential. Staining for broad cell cycle and mitosis markers, Ki67 and Aurkb, revealed a reduction in cell cycle activity for the phospho-mutants and particularly for the YAP2A mutant for ERBB2-mediated CM mitosis (Fig. 5H-J). Overall, these findings demonstrate the requirement of YAP phosphorylation on S274 and S352 during CM mitosis. Apart from mitosis, the phosphorylation of YAP on S274 is strongly associated with the altered

cytoskeleton in OE CMs, correlative with YAP activation.

Discussion

In this study we have asked what underlies the potent regenerative outcome of transient ERBB2 signaling in adult mouse CMs. We revealed a crosstalk between the two major signaling hubs in CMs, ERBB2 and YAP, and present numerous novel insights in the field of cardiac regeneration. We demonstrate that even a scarred heart (HF model) is amenable to regeneration by activated myocardial ERBB2 signaling, a notion that has only recently sprouted in the field of cardiac regeneration[16]. Our study demonstrates core EMT-like processes during cardiac regeneration, beyond CM dedifferentiation and proliferation. The emerging massive ECM and cytoskeletal remodeling coupled with CM migration seems to be pivotal for scar replacement by new CMs. This is in line with other studies suggesting that CM migration is essential for cardiac regeneration[50,51,15].

Mature CMs are highly specialized, stationary and strongly coupled to each other, an un-intuitive cell for EMT-like behaviors. In the embryo, processes which recapitulate core-EMT behaviors are essential to proper cardiac development and morphogenesis[52,53,54,55]. We show that ERBB2 activation coerces adult CMs to become more fibroblast- and embryonic- like in nature, performing competitively in the context of existing fibrosis by movement, proliferation and engagement with the ECM. The EMT-like features seen in OE CMs are accompanied by robust changes in the cytoskeletal infrastructure, which underlies their biology. This also reflects a high degree of dedifferentiation, reminiscent (at least in part) of embryonic and cancerous processes[54], illustrating that the underlying mechanisms of malignancy, development and regeneration may ‘draw from the same deck’. Concomitantly, this also highlights the importance of the transience (i.e. eventual cessation) of the oncogenic signaling for functional rebound[56].

We demonstrated the involvement of YAP signaling downstream of ERBB2 in CMs, and its requirement for various ERBB2-related phenotypes. We present evidence that YAP activation occurs in the context of, and in association with, the altered cytoskeletons. YAP binding partners associated with cytoskeletal and nuclear envelope compartments, force sensors upregulation and nuclear shearing all suggest that ERBB2 signals to YAP is mediated via cytoskeleton to the nucleus. Although key studies in the field of YAP mechanical regulation focus on actomyosin-driven mechanical relay[22,57,58,59], our Co-IP assay detected novel associations of YAP with the cardiac embryonic intermediate filament Nestin and other

sarcomeric modulators. In line with our findings, pYAP S274 and pYAP S352 were detected (together or alone) in several reports as being phosphorylated during mitosis[60,47,61]. We show that the phosphorylation at those sites is required for mitosis, and is conserved among other proliferative CM systems, as in the case of embryonic CMs or adult CMs derived from YAP5SA mice[17].

To conclude, we reveal a novel ERBB2-YAP signaling relay based on cytoskeleton remodeling which regulates CM division and EMT-like processes during cardiac regeneration.

Author contributions

A.A. and E.T. conceived and designed the experiments. A.A with help from A. Shakked carried out most of the experiments and analyzed the data. Specifically, A. Shakked helped with animal studies, tissue culture work, RT-PCR, and cloning of YAP mutants into AAV viruses and all revolving work and analysis. K.B.U. helped with animal studies, RNA - seq preparation and analysis and enabled the simultaneous RNA, protein and phosphoprotein acquisition method for HTS used throughout this study. A. Savidor and Y.L performed proteomic analysis. D.K. and D.L. performed MI and echocardiographic analysis. O-Y.R helped with functional gelatin degradation assays and migration time-lapse microscopy. Y.M helped with 5SA heart sections. J.D. provided custom made and pYAP S274 antibody. B.G and J.F.M contributed to the planning and progression of the project. E.T supervised the entire project. A.A and E.T wrote the manuscript with editing contributions from all the authors.

Acknowledgments

This study has been supported by grants to E.T from the European Research Council (ERC StG #281289, CM turnover, and ERC AdG #788194, CardHeal), the U.S.-Israel Binational Science Foundation (BSF) to both E.T. and J.F.M., the Israel Science Foundation (ISF), Foundation Leducq Transatlantic Network of Excellence, and Minerva foundation with funding from the Federal German Ministry for Education and Research. This work was supported by grants from the National Institutes of Health (HL127717, HL130804, HL118761 (J.F.M.); Vivian L. Smith Foundation (J.F.M.), State of Texas funding (J.F.M.). We thank Dr. Oded Singer for help with AAV preps and shared materials, Dr. Gilgi Friedlander for RNAseq analysis and inputs, and Noam Priel for teaching ‘trackmate’ software usage.

References

1. Tzahor, E. & Poss, K. D. Cardiac regeneration strategies: Staying young at heart. **1039**, 1035–1039 (2017).

2. Poss, K. D., Wilson, L. G. & Keating, M. T. Heart regeneration in zebrafish. *Science* **298**, 2188–90 (2002).

3. Porrello, E. R. *et al.* Transient regenerative potential of the neonatal mouse heart. *Sci. New York NY* **331**, 1078–80 (2011).

4. Jopling, C. *et al.* Zebrafish heart regeneration occurs by cardiomyocyte dedifferentiation and proliferation. *Nature* **464**, 606–9 (2010).

5. Leone, M. & Engel, F. B. Advances in heart regeneration based on cardiomyocyte proliferation and regenerative potential of binucleated cardiomyocytes and polyploidization. 1229–1253 (2019).

6. Sadek, H. & Olson, E. N. Toward the Goal of Human Heart Regeneration. *Cell Stem Cell* **26**, 7–16 (2020).

7. Itou, J. *et al.* Migration of cardiomyocytes is essential for heart regeneration in zebrafish. *Development* **139**, 4133–4142 (2012).

8. Harvey, R. P., Wystub-Lis, K., del Monte-Nieto, G., Graham, R. M. & Tzahor, E. Cardiac Regeneration Therapies - Targeting Neuregulin 1 Signalling. *Hear. Lung Circ.* **25**, 4–7 (2016).

9. D'Uva, G. *et al.* ERBB2 triggers mammalian heart regeneration by promoting cardiomyocyte dedifferentiation and proliferation. *Nat. Cell Biol.* **17**, 627–638 (2015).

10. Gemberling, M., Karra, R., Dickson, A. L. & Poss, K. D. Nrg1 is an injury-induced cardiomyocyte mitogen for the endogenous heart regeneration program in zebrafish. *Elife* **4**, 1–17 (2015).

11. Polizzotti, B. D. *et al.* Neuregulin stimulation of cardiomyocyte regeneration in mice and human myocardium reveals a therapeutic window. *Sci. Transl. Med.* **7**, 281ra45 (2015).

12. Heallen, T. *et al.* Hippo pathway inhibits Wnt signaling to restrain cardiomyocyte proliferation and heart size. *Science* **332**, 458–61 (2011).

13. Wang, J., Liu, S., Heallen, T. & Martin, J. F. The Hippo pathway in the heart: pivotal roles in development, disease, and regeneration. *Nat. Rev. Cardiol.* **15**, 672–684 (2018).

14. Heallen, T. *et al.* Hippo signaling impedes adult heart regeneration. *Development* **140**, 4683–90 (2013).

15. Morikawa, Y. *et al.* Actin cytoskeletal remodeling with protrusion formation is essential for heart regeneration in Hippo-deficient mice. *Sci. Signal.* **8**, 1–14 (2015).

16. Heallen, T. *et al.* Hippo pathway deficiency reverses systolic heart failure after infarction. *Nat. Publ. Gr.* **550**, 260–264 (2017).

17. Monroe, T. O. *et al.* YAP Partially Reprograms Chromatin Accessibility to Directly Induce Adult Cardiogenesis In Vivo. *Dev. Cell* **48**, 765-779.e7 (2019).

18. von Gise, A. *et al.* YAP1, the nuclear target of Hippo signaling, stimulates heart growth through cardiomyocyte proliferation but not hypertrophy. *Proc. Natl. Acad. Sci. U. S. A.* **109**, 2394–9 (2012).

19. Xin, M. *et al.* Regulation of IGF signalling by YAP Governs Cardiomyocyte proliferation and Embryonic Heart Size. **4**, 1–15 (2012).

20. Xin, M. *et al.* Hippo pathway effector Yap promotes cardiac regeneration. *Proc. Natl. Acad. Sci.* **110**, 13839–13844 (2013).

21. Panciera, T., Azzolin, L., Cordenonsi, M. & Piccolo, S. Mechanobiology of YAP and TAZ in physiology and disease. *Nat. Rev. Mol. Cell Biol.* **18**, 758–770 (2017).

22. Dupont, S. *et al.* Role of YAP/TAZ in mechanotransduction. *Nature* **474**, 179–183 (2011).

23. Ragni, C. V. *et al.* Amotl1 mediates sequestration of the Hippo effector Yap1 downstream of Fat4 to restrict heart growth. *Nat. Commun.* **8**, 14582 (2017).

24. Hirai, M. *et al.* Adaptor proteins NUMB and NUMBL promote cell cycle withdrawal by targeting ERBB2 for degradation. **127**, 569–582 (2017).

25. Li, J. *et al.* Alpha-catenins control cardiomyocyte proliferation by regulating yap activity. *Circ. Res.* **116**, 70–79 (2015).

26. Nakada, Y. *et al.* Hypoxia induces heart regeneration in adult mice. *Nature* 1–21

(2016). doi:10.1038/nature20173

27. Marín-juez, R. *et al.* Fast revascularization of the injured area is essential to support zebrafish heart regeneration. *Proc. Natl. Acad. Sci.* **113**, 11237–11242 (2016).

28. Das, S. *et al.* A Unique Collateral Artery Development Program Promotes Neonatal Heart Regeneration. *Cell* **176**, 1128-1142.e18 (2019).

29. Honkoop, H. *et al.* Single-cell analysis uncovers that metabolic reprogramming by ErbB2 signaling is essential for cardiomyocyte proliferation in the regenerating heart. *Elife* 1–65 (2019).

30. Fukuda, R. *et al.* Metabolic modulation regulates cardiac wall morphogenesis in zebrafish. *Elife* (2019).

31. Lamouille, S., Xu, J. & Derynck, R. Molecular mechanisms of epithelial–mesenchymal transition. *Nat. Rev. Mol. Cell Biol.* **15**, 178–196 (2014).

32. Zhao, B. *et al.* Inactivation of YAP oncoprotein by the Hippo pathway is involved in cell contact inhibition and tissue growth control. *Genes Dev.* **21**, 2747–2761 (2007).

33. Zhao, B., Li, L., Tumaneng, K., Wang, C. Y. & Guan, K. L. A coordinated phosphorylation by Lats and CK1 regulates YAP stability through SCFβ-TRCP. *Genes Dev.* **24**, 72–85 (2010).

34. Ni, L., Zheng, Y., Hara, M., Pan, D. & Luo, X. Structural basis for Mob1-dependent activation of the core Mst – Lats kinase cascade in Hippo signaling. *Genes Dev.* **29**, 1416–1431 (2015).

35. Zhao, B. *et al.* Inactivation of YAP oncoprotein by the Hippo pathway is involved in cell contact inhibition and tissue growth control. *Genes Dev.* **21**, 2747–2761 (2007).

36. Leber, Y. *et al.* Filamin C is a highly dynamic protein associated with fast repair of myofibrillar microdamage. **25**, 2776–2788 (2016).

37. Juo, L.-Y. *et al.* HSPB7 interacts with dimerized FLNC and its absence results in progressive myopathy in skeletal muscles. *J. Cell Sci.* **129**, 1661–1670 (2016).

38. Scheffer, D. I. *et al.* XIRP2, an actin-binding protein essential for inner ear hair-cell stereocilia. *Cell Rep.* **10**, 1811–1818 (2015).

39. Hertig, V. *et al.* Nestin expression is dynamically regulated in cardiomyocytes during

embryogenesis. *J. Cell. Physiol.* **233**, 3218–3229 (2018).

40. Stroud, M. J., Banerjee, I., Veevers, J. & Chen, J. LINC complex proteins in cardiac structure, function, and disease. *Circ Res.* **31**, 538–548 (2014).

41. Kirby, T. J. & Lammerding, J. Emerging views of the nucleus as a cellular mechanosensor. *Nat. Cell Biol.* **20**, 373–381 (2018).

42. Swift, J. *et al.* Nuclear lamin-A scales with tissue stiffness and enhances matrix-directed differentiation. *Science (80-.).* **341**, 965–966 (2013).

43. Cho, S., Irianto, J. & Discher, D. E. Mechanosensing by the nucleus: From pathways to scaling relationships. *J. Cell Biol.* **216**, 305–315 (2017).

44. Torvaldson, E., Kochin, V. & Eriksson, J. E. Phosphorylation of lamins determine their structural properties and signaling functions. *Nucleus* **6**, 166–171 (2015).

45. Delmar, M. & Liang, F.-X. Connexin43, and the regulation of intercalated disc function. *Hear. Rhythm.* **9**, 835–838 (2012).

46. Robison, P. *et al.* Detyrosinated microtubules buckle and bear load in contracting cardiomyocytes. *Science (80-.).* **352**, aaf0659 (2016).

47. Yang, S. *et al.* CDK1 phosphorylation of YAP promotes mitotic defects and cell motility and is essential for neoplastic transformation. *Cancer Res.* **73**, 6722–6733 (2013).

48. Lin, Z. & Pu, W. T. Releasing YAP from an α-catenin trap increases cardiomyocyte proliferation. *Circulation Research* **116**, 9–11 (2015).

49. Morikawa, Y., Heallen, T., Leach, J., Xiao, Y. & Martin, J. F. Dystrophin–glycoprotein complex sequesters Yap to inhibit cardiomyocyte proliferation. *Nat. Publ. Gr.* **547**, 227–231 (2017).

50. Zhang, R. *et al.* In vivo cardiac reprogramming contributes to zebrafish heart regeneration. *Nature* **498**, 497–501 (2013).

51. Tahara, N., Brush, M. & Kawakami, Y. Cell migration during heart regeneration in zebrafish. *Developmental Dynamics* **245**, 774–787 (2016).

52. del Monte-Nieto, G. *et al.* Control of cardiac jelly dynamics by NOTCH1 and NRG1 defines the building plan for trabeculation. *Nature* **557**, 439–471 (2018).

53. Von Gise, A. & Pu, W. T. Endocardial and epicardial epithelial to mesenchymal transitions in heart development and disease. *Circ. Res.* **110**, 1628–1645 (2012).

54. Nieto, M. A., Huang, R. Y. Y. J., Jackson, R. A. A. & Thiery, J. P. P. Emt: 2016. *Cell* **166**, 21–45 (2016).

55. Combs, M. D. & Yutzey, K. E. Heart Valve Developement: Regulatory Networks in Development and Disease AV. **105**, 933–942 (2009).

56. Gabisonia, K. *et al.* MicroRNA Therapy stimulates uncontrolled cardiac repair after myocardial infarction in pigs. *Nature* **569**, (2019).

57. Aragona, M. *et al.* A mechanical checkpoint controls multicellular growth through YAP/TAZ regulation by actin-processing factors. *Cell* **154**, 1047–1059 (2013).

58. Elosegui-Artola, A. *et al.* Force Triggers YAP Nuclear Entry by Regulating Transport across Nuclear Pores. *Cell* **171**, 1397-1410.e14 (2017).

59. Shiu, J. Y., Aires, L., Lin, Z. & Vogel, V. Nanopillar force measurements reveal actin-cap-mediated YAP mechanotransduction. *Nat. Cell Biol.* **20**, 1–10 (2018).

60. Bui, D. A. *et al.* Cytokinesis involves a nontranscriptional function of the Hippo pathway effector YAP. *Sci. Signal.* **9**, ra23–ra23 (2016).

61. Zhao, Y. *et al.* YAP-induced resistance of cancer cells to antitubulin drugs is modulated by a hippo-independent pathway. *Cancer Res.* **74**, 4493–4503 (2014).

Fig. 1: Delayed ERBB2 activation in CMs triggers functional recovery, scar replacement and involves EMT-like processes

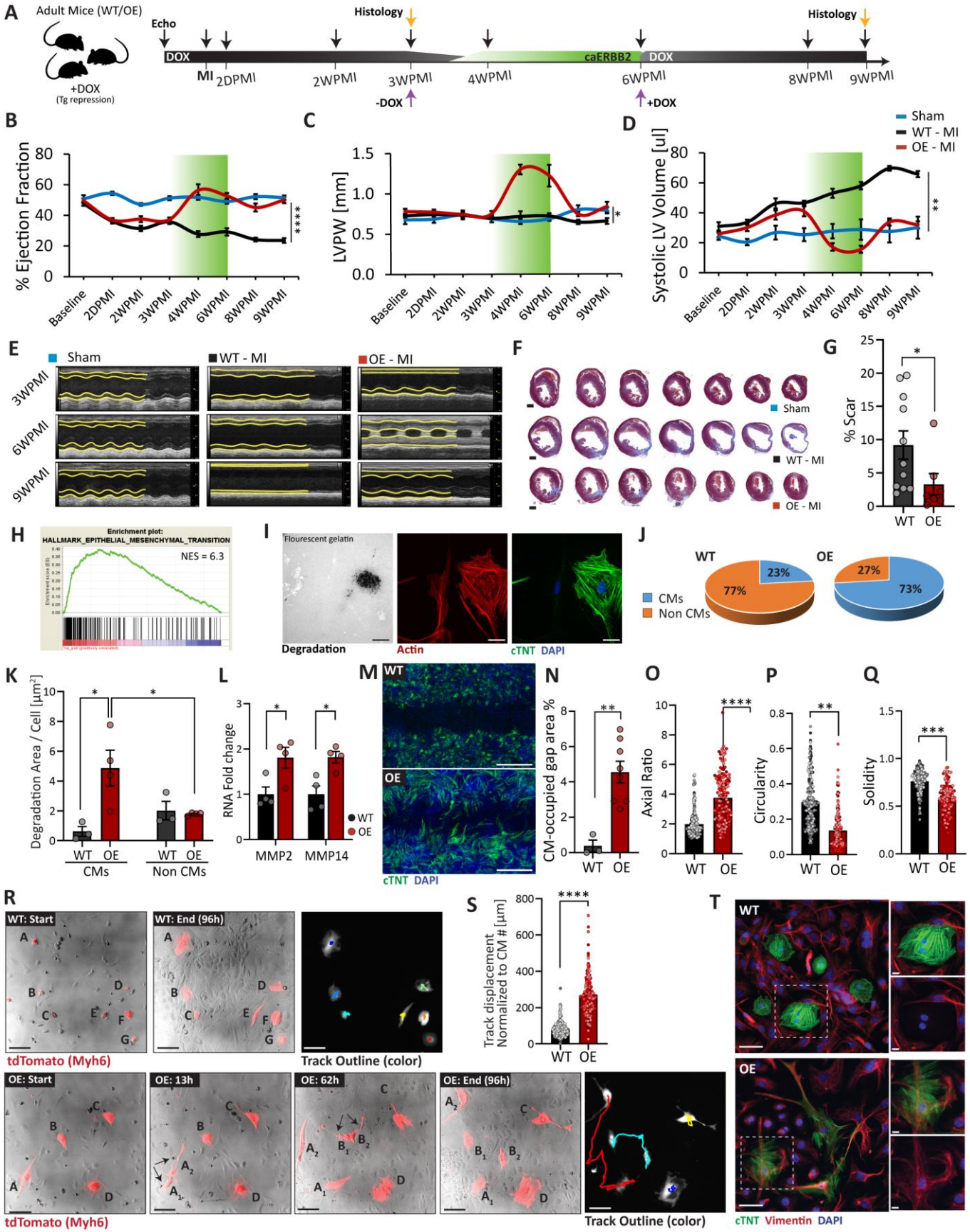

(A) A diagram describing the experimental outline in adult mice of transient ca*Erbb2* over expression. Mice were subjected to LAD ligation (Myocardial infarction, MI), and caErbb2 induction was started 3weeks post MI (3WPMI), up to 6WPMI. Purple arrows indicate removal and re-instatement of DOX diet resulting in approximately 2.5weeks period of caErbb2 expression denoted as a green bar. Black arrows indicate Echo measurements. Orange arrows indicate histological analysis. (B-D) graphic representation of cardiac parameters derived from echocardiographic imaging analysis, performed at the indicated time points in (A). n=16 mice for WT, n=11 mice for OE, n=5 for Sham; (B) Cardiac ejection fraction %. (C) left ventricular posterior wall (LVPW) thickness. (D) Systolic left ventricular (LV) volume. (E) Representative M-mode images of anterior and posterior wall contractility for Sham, WT-MI and OE-MI, at the indicated time points. (F) Representative transverse histological sections of Sham, WT and OE hearts 9 weeks after injury stained for Masson's trichrome showing scarring in blue. Scale bars, 1 mm. (G) Scar quantification (%) for data in (F). n=11 mice for WT, n=7 for OE. Significance was determined by one-tailed t-test. (H) Bulk RNA - seq WT-MI and OE-MI analysed using GSEA hallmark module. Representative image of gene contribution to epithelial to mesenchymal transition hallmark. (I) Immunofluorescence (IF) of indicated proteins showing degradation (black, loss of signal) in the gelatin channel co-localizing to a CM (positive for cTNT) in the perinuclear area. Scale bars, 25 µm. (J) Analysis of the proportion of degradation area in P7 cardiac cultures divided between CMs and non-CMs for OE and WT P7 cardiac cultures. (K) The specific degradation area normalized per cell for CMs and non-CMs in OE and WT P7 cardiac cultures. (n=56 CM, n=676 non-CM for WT, n=91 CMs n=680 non-CMs for OE). (L) qRT-PCR analysis of *MMP2* and *MMP14* transcripts in OE-MI and WT-MI adult heart lysates. (n=4 for WT, and n=4 for OE). (M) IF staining for the indicted proteins in a migration assay for P7 WT and OE cardiac cultures 4 days after barrier removal. Scale bars, 500 µm. (N) Quantification of CM-occupied gap area % in (M) (n=3 for WT, n=8 for OE). (O) Axial ratio quantification of OE and WT P7 CMs as a proxy for morphological changes (elongation in a particular axis) (n= 183 for WT, n=131 for OE). (P) Circularity quantification of OE and WT P7 CMs as a proxy for morphological changes. (n= 183 for WT, n=131 for OE). (Q) Solidity quantification of OE and WT P7 CMs as a proxy for morphological changes (protrusions and indentations). (n= 183 for WT, n=131 for OE). Bars are comprised of colour coded dots that differentiate data points derived from different biological repeats for (O-Q). (R) Representative images for the migration movies for WT and OE P7 cardiac cultures with CMs tagged with endogenous tdTomato fluorescent protein. The timing of each picture is

denoted, arrows indicate mitosis and letters indicate specific cells throughout the images. Track outline indicates in color the individual displacement of a cell during the movie. Scale bars, 50 µm. (S) Track displacement normalized to CM number that make up a particular track in (R) plotted for WT and OE CMs. Bars are comprised of color coded dots that differentiate data points derived from different biological repeats. (n =190 for WT and n=175 for OE). (T) IF staining for the indicated proteins in P7 cardiac cultures of WT/OE. Scale bars, 50 µm. Insets are enlarged to the right. Inset Scale bars, 10 µm.
*$p < 0.05$; **$p < 0.01$; ***$p < 0.001$; ****$p<0.0001$. Error bars indicate SEM. All experiments were performed for at least 3 biological repeats.

Fig. 2: YAP is activated downstream to ERBB2 signaling in CMs

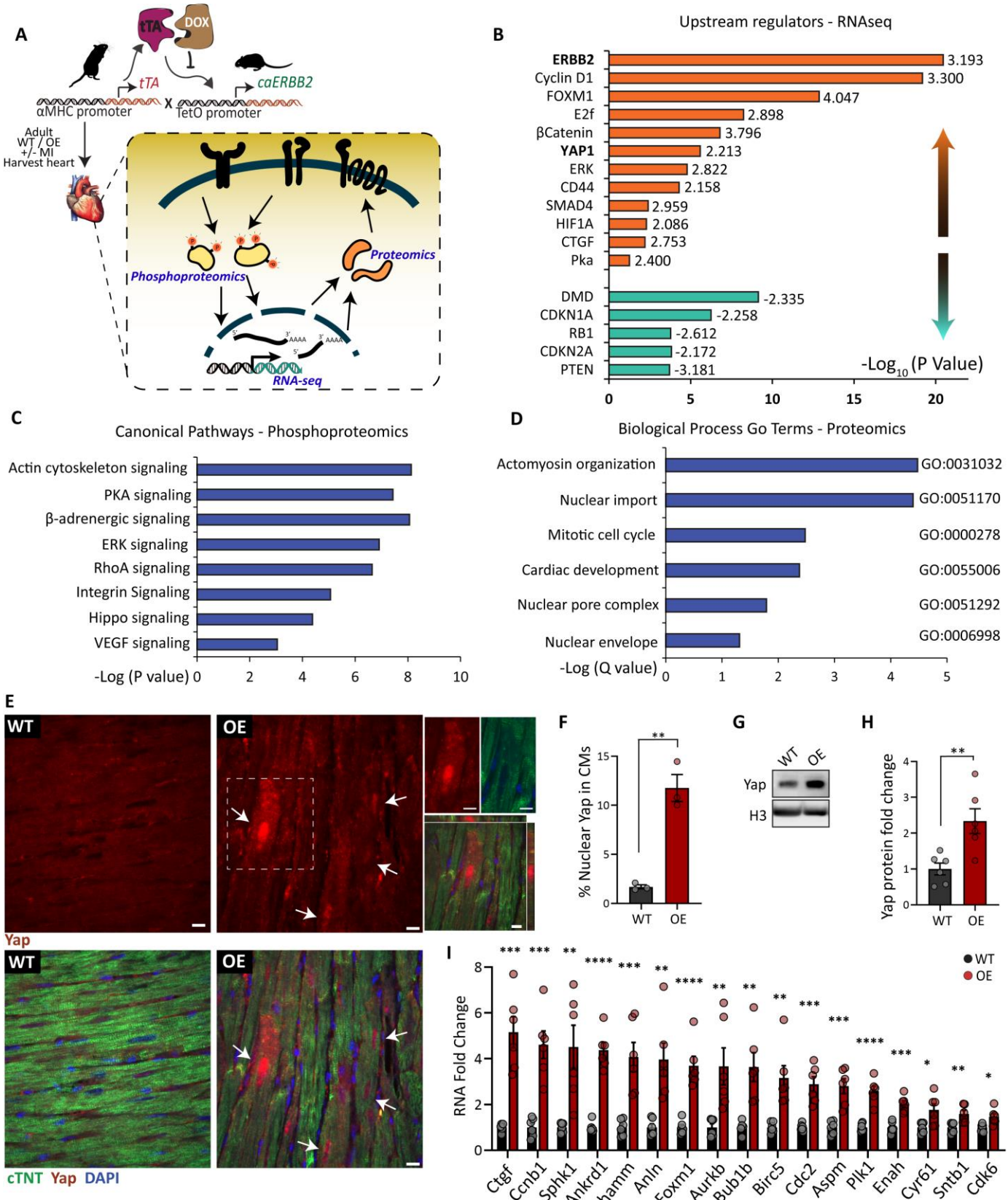

(A) A Scheme representing the genetic model, experimental setup and assays employed. Hearts of adult WT and OE (Sham/ MI) were harvested 2 weeks after DOX removal. RNA and protein samples were simultaneously collected for RNA-seq, proteomics and phosphoproteomics analysis. n=4 for WT Sham, n=4 for WT-MI, n=4 for OE Sham, n=4 for OE-MI. (B) Predicted upstream regulators (IPA software) of differentially expressed genes between OE-MI and WT-MI RNA –seq datasets, using a threshold FC≥1.5, p adjusted ≤0.05. Indicated number to the right is z-score for activation (>2) or inhibition (<2). (C) Clustering of differentially phosphorylated proteins (p-value ≤ 0.05) between OE-MI and WT-MI to canonical pathways (regardless of phosphorylation) analyzed by IPA. (D) GO Clustering of differentially expressed proteins for biological processes category using PANTHER software. Marks next to bar represent GO term codes. (E) IF of indicated proteins in WT/OE heart sections. Arrows point to nuclear accumulation of Yap. Scale bar, 10 µm. Upper insets show a disrupted cTNT pattern concomitant with Yap cytoskeletal presence. Lower inset shows a z-stack image of Yap nuclear penetration. Scale bars, 10 µm. Images were taken in and around the border zone. (F) Quantification of IF in (E). Yap regarded as nuclear if the nuclear intensity was stronger than the cytoplasmic (n=1246 CMs for WT and n=713 CMs for OE). (G) WB analysis of Yap levels from in vivo adult WT/OE heart lysates. (H) Quantification of (G) (n=6 for WT and n=6 for OE). (I) qRT-PCR analysis of Yap target genes in OE/WT hearts (n=6 for WT, n=6 for OE).

*$p < 0.05$; **$p < 0.01$; ***$p < 0.001$; ****$p<0.0001$. Error bars indicate SEM. All experiments were performed for at least 3 biological repeats.

Fig. 3: YAP is required for ERBB2-related cardiac phenotypes

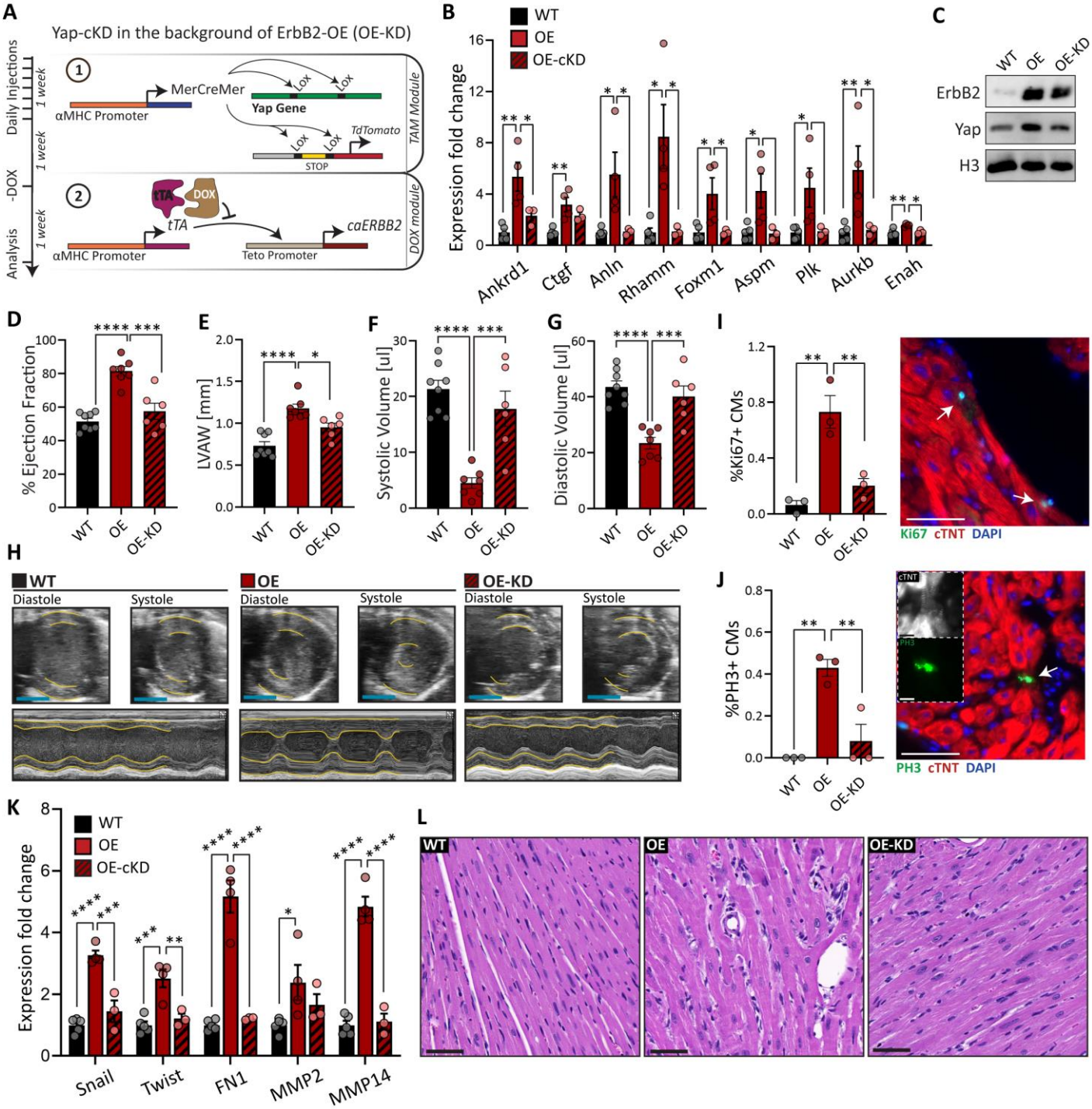

(A) Schematic illustration of the OE-KD mouse model and induction regimes for Tamoxifen (TAM) and doxycycline (DOX), controlling Yap deletion and caErbB2 over expression, respectively. Conditional Yap deletion was done by 7 consecutive Tam injections, and after another week we induced caErbb2 by Dox removal for an additional week. (B) qRT- PCR analysis of Yap target genes in WT, OE and OE-KD heart lysates (n=5 for WT, n=4 for OE, and n=3 for OE-KD). (C) WB analysis of the indicated proteins from in vivo adult WT, OE

and OE-KD heart lysates. (D-G) cardiac parameters acquired from echocardiography analysis, comparing WT, OE and OE-KD mice. n=8 mice for WT, n=7 mice for OE, n=6 for OE-KD; (D) Ejection fraction % ; (E) Left ventricular anterior wall (LVAW) Thickness; (F) Systolic volume (G) Diastolic volume ; (H) M-mode representative images of heart in diastole and systole. Yellow tracing reflects of anterior and posterior wall contractility, for WT, OE and OE-KD mice. (I) IF analysis of % Ki67 positive CMs for WT, OE and OE-KD heart sections. Scale bar 50 µm. Arrows point to $Ki67^{+}$ CM. (J) IF analysis of %PH3 positive CMs for WT, OE and OE-KD heart sections. Scale bar 50 µm. Arrow points to $PH3^{+}$ CM (in metaphase). Insets highlight the disrupted sarcomere in the cTNT channel in grey (upper) and the condensed chromatin marked with PH3 with green (bottom). Scale bar 10 µm. (K) qRT-PCR analysis of EMT hallmark genes in WT, OE and OE-KD heart lysates (n=5 for WT, n=4 for OE, and n=3 for OE-KD). (L) Haematoxylin and Eosin stained histological sections of WT, OE and OE-KD hearts. Scale bar 50 µm.

*$p < 0.05$; **$p < 0.01$; ***$p < 0.001$; ****$p<0.0001$. Error bars indicate SEM. All experiments were performed for at least 3 biological repeats.

Fig. 4: ERBB2 signaling induces an altered mechanical state in CMs

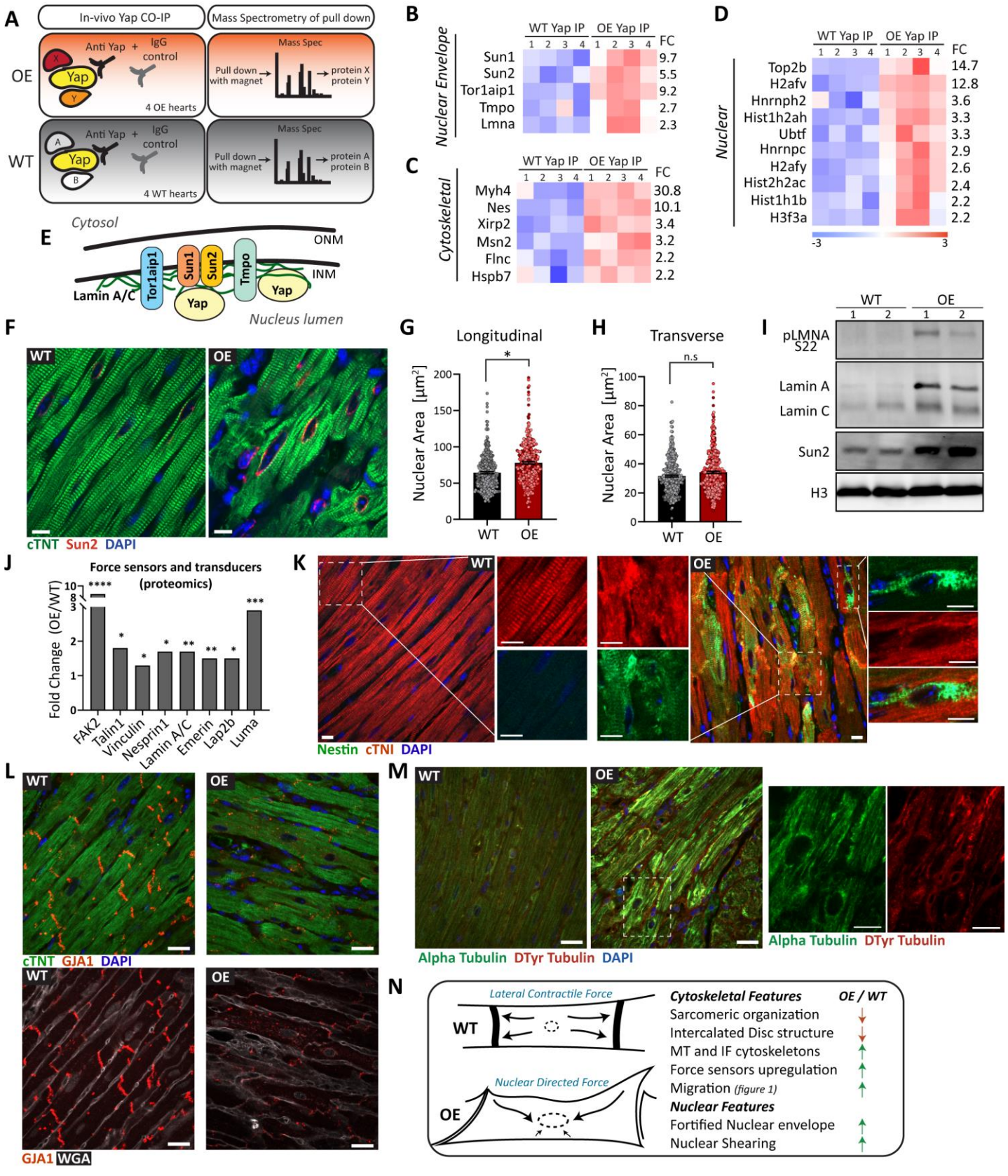

(A) Schematic illustration of Co-IP-MS experiment (n=4 IP reactions in WT, n=4 IgG reactions in WT, n=4 IP reactions in OE, n=4 IgG reactions in OE). (B) Heat map of Yap binding partners from the nuclear envelope, cytoskeleton (C), and nucleus (D). For panels (B-D) FC to the right indicates fold change of the detected protein by Mass Spec. All displayed results are at p-value ≤ 0.05. Full binding partner list appears at Figure S4. (E) Illustration of Yap associated proteins from (B) that can complex together at the inner nuclear membrane (INM). (F) IF analysis of heart sections for the indicated proteins. Scale bar 10µm. (G) Quantification of CM nuclei cross-sectional area from (F) in longitudinally cut CMs (n=313 for WT, n=361 for OE), and in transversely cut CMs (n=349 for WT, n=394 for OE) in (H). For panels (G-H) Bars are comprised of color coded dots that differentiate data points derived from different biological repeats. (I) WB analysis of the indicated protein in adult WT/OE heart lysates. (J) Proteomic data of OE/WT fold change of the indicated proteins (n=4 hearts for WT, n=4 hearts for OE). (K) IF analysis of heart sections for the indicated proteins for a WT/OE. Insets show separately two of the channels to illustrate the structural disassembly of cTNI and Nestin accumulation in OE hearts compared to WT. Scale bar 10µm. (L) IF analysis of heart sections for the indicated proteins for a WT/OE. Scale bar 10µm. (M) IF analysis of heart sections for the indicated proteins for a WT/OE. Inset of the OE image shows separately two of the channels. Scale bar 10µm. (N) Scheme summarizing differences in force distribution between a WT/OE CMs based on nuclear and cytoskeletal parameters. $*p < 0.05$; $**p < 0.01$; $***p < 0.001$; $****p<0.0001$. Error bars indicate SEM. All experiments were performed for at least 3 biological repeats.

Fig. 5: YAP phosphorylation on S274 and S352 peaks during metaphase, and is required for cell division

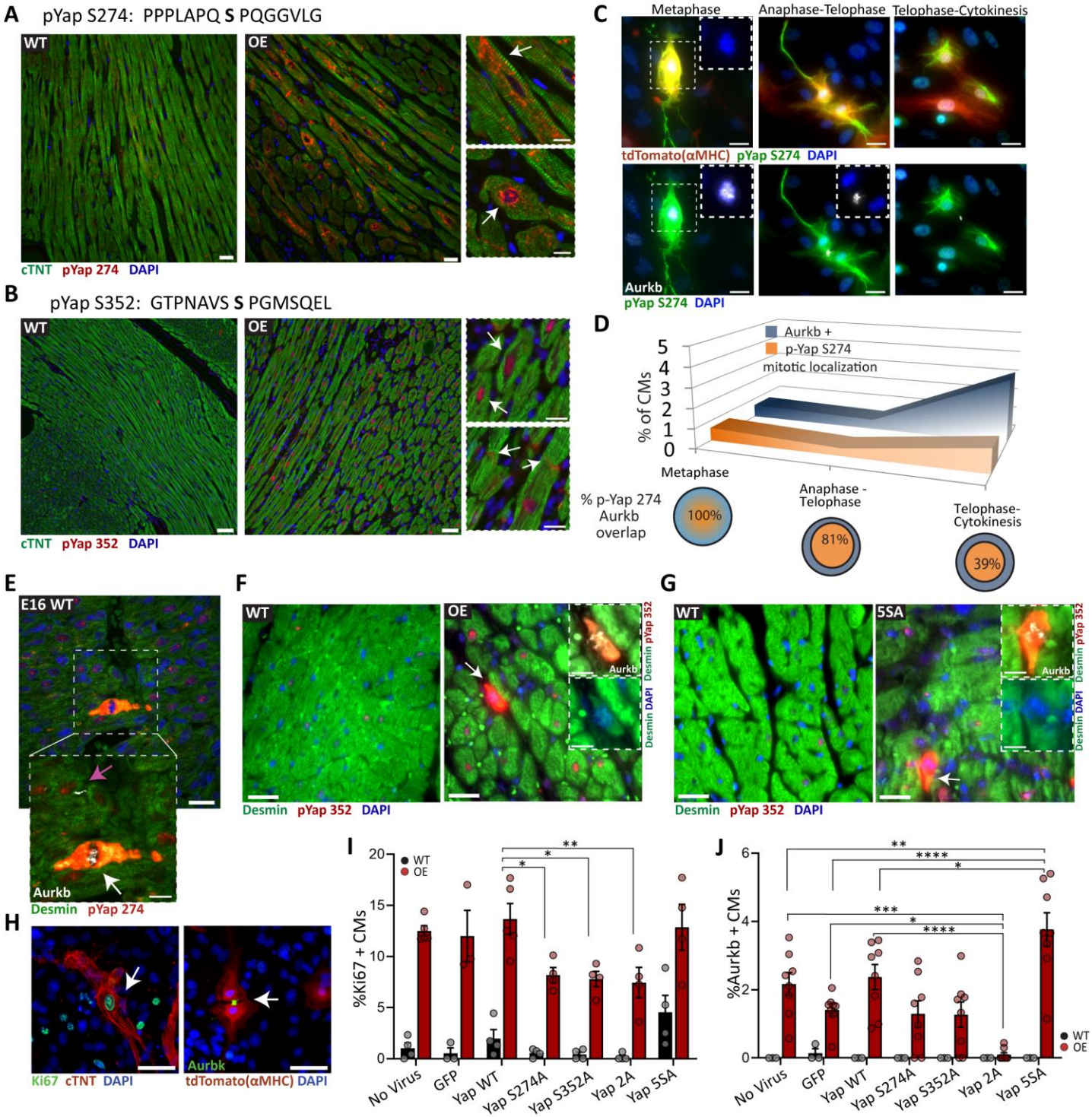

(A) Upper: Phosphorylation of highlighted serine on Yap identified by Yap-IP-MS (Figure 4A) enriched in OE adult heart lysates (*pv* <0.05). Lower: IF analysis of adult heart sections of the indicated proteins for WT/OE. Scale bar 20µm. Upper inset depicts the cytoskeletal morphology abundant in OE CMs, lower inset depicts the nuclear (and nuclear envelope) morphology abundant in OE CMs. Scale bar 10µm. (B) Upper: Phosphorylation of

highlighted serine on Yap identified by MS phosphosproteomic analysis (Figure 2A) enriched in OE adult heart lysates (pv <0.05). Lower: IF analysis of adult heart sections of the indicated proteins for WT/OE. Scale bar 50µm. Upper inset depicts the nuclear accumulation abundant in OE CMs, lower inset shows the presence in intercalated discs. Scale bar 20µm. (C) Representative IF images for the indicated proteins at the metaphase, anaphase-telophase and telophase-cytokinesis stages in P7 OE cardiac cultures (CM lineage endogenously tagged with tdTomato). Scale bar 20µm. (D) Quantification of CMs positive for Aurkb (blue curve) and pYap S274 mitotic peak localization (orange curve) counted at the different stages of mitosis plotted on the x axis. Bottom: Venn diagram show the degree of overlap between of pYap S274 mitotic peak localization from all Aurkb events. (n=2327 CMs) (E) IF analysis of embryonic WT E16.5 heart sections for the indicated proteins. Lower inset shows selected area counterstained with Aurkb. White arrow points to a CM in metaphase and pink arrow points to cytokinesis. Scale bar 10µm. (F) Immunofluorescence analysis of heart sections for the indicated proteins for WT/OE. Scale bar, 25µm. OE Insets show, with different channels, a CM in metaphase. Scale bar, 10µm. (G) IF analysis of heart sections for the indicated proteins for WT/5SA. Scale bar, 25µm. 5SA Insets show, with different channels, a CM in metaphase. Scale bar, 10µm. (H-J) WT/OE P7 cardiac cultures infected with the indicated AAV viruses, and stained for cell cycle markers Ki67 and Aurkb; (H) Representative IF images of CMs positive for Ki67 and Aurbk. Scale bar, 50µm. (I) Quantification of the Ki67% positive CMs (n= 3454 CMs for WT, n=6482 CM for OE), and (J) Aurkb% positive CMs (n= 2576 CMs for WT, n=12615 CM for OE). Signal for Aurkb was considered positive from metaphase onwards. *p < 0.05; **p < 0.01; ***p < 0.001; ****p<0.0001. Error bars indicate SEM. All experiments were performed for at least 3 biological repeats.